Journal of Materials Chemistry C

Accepted Manuscript

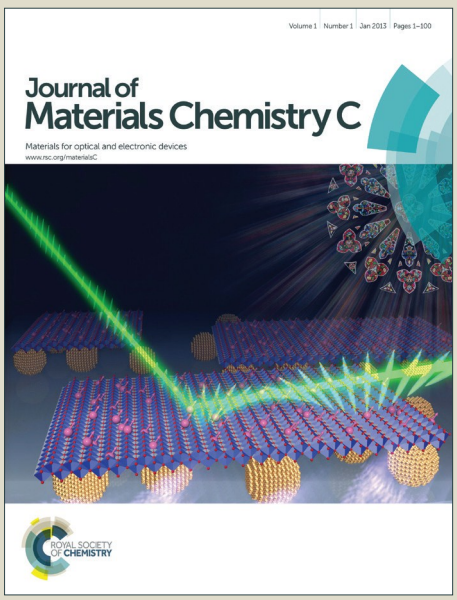

ROYAL SOCIETY OF CHEMISTRY

www.rsc.org/materialsC

Journal Name

RSCPublishing

ARTICLE

Nanofibers generated from nonclassical organogelators based on difluoroboron β-diketonate complexes to detect aliphatic primary amine vapors

Cite this: DOI: 10.1039/x0xx00000x

Received 00th January 2012,
Accepted 00th January 2012

DOI: 10.1039/x0xx00000x

www.rsc.org/

Lu Zhai,[a] Mingyang Liu,[a] Pengchong Xue,[a] Jingbo Sun,[a] Peng Gong,[a] Zhenqi Zhang,[a] Jiabao Sun[a] and Ran Lu[*a]

New D-A-D type difluoroboron β-diketonate complexes with terminal triphenylamines **ABA**, **ABVA** and **AVBVA** were synthesized. It was found that the stable organogels could be gained from **ABVA** and **AVBVA** without traditional gelation groups in the mixed solvents containing 1,4-dioxane, and the balanced π-π interactions were the driving forces for the gel formation. Interestingly, the organogels based on **ABVA** and **AVBVA** exhibited the emission closing to NIR (near infrared) region. To the best of our knowledge, such narrow band gap low molecular-weight π-gelator has not been reported. In particular, the xerogel-based films generated from **ABVA** and **AVBVA** could be used as sensors to detect gaseous aliphatic primary amines with high performance. For example, exposing to saturated *n*-butylamine and *n*-propylamine vapors for 30 s, the emission of the films was quenched completely and new strong emission at ca. 560 nm appeared on account of the decomposition of the difluoroboron β-diketonate complexes.

Introduction

Detection of volatile organic amines is of great interest in the fields of environmental pollution monitoring and control, food safety, and even medical diagnosis.[1-9] To date, some approaches for detecting organic amines, such as electrochemical devices,[10] gas or liquid chromatography,[11] and various chemical sensors,[12] have been employed. Particularly, fluorescent sensors for detecting amines have received much attention because of high sensitivity, high selectivity, local observation and remote sensing.[13] Recently, some sensory materials based on self-assembled fluorescent fibrous films have been developed for detecting organic amine vapors due to their high sensitivity. For example, Zang and co-workers have reported a sensor based on nanofibers fabricated from *n*-type organic semiconductor for detecting organic amine vapors.[14,15] Mohr et al. have employed fluorescent dye-based membranes for probing lipophilic primary amines with high sensitivity and selectivity via reversible chemical reactions.[16,17] Fang and co-workers have reported an ultrasensitive fluorescent sensing film based on cholesterol-modified perylene bisimide for detecting organic amines.[18] Our group also developed emitting fibrous-based films fabricated from boron diketonate complexes for probing organic amines.[19] We have found that the conjugated molecules with V-shaped π-skeleton preferred to self-assemble into 1D nanofibers in an organogel phase directed by balanced (neither too strong nor too weak) π-π interactions,[20c] and the fluorescent organogel nanofibers-based films could become good candidate in sensory materials.[19b] Although the organogelation of π-gelators became a facile approach to fabricate functional organic nanostructures, the gelators without traditional gelation groups (such as long carbon chain, cholesterol, hydrogen-bonded units, etc.) were seldom reported.[20] On the one hand, the preparation of nonclassical organogelators without traditional gelation groups would fulfill the atom economy in the synthesis. On the other hand, the obstacles of the information transformation between conjugated systems would be avoided because of the absence of the domain formed from long carbon chains. Previously, we have found that the difluoroboron β-diketonate complexes with V-shaped conjugated skeleton exhibited good gelation ability.[20c] With this in mind, we synthesized new V-shaped triphenylamine functionalized difluoroboron β-diketonate complexes **ABA**, **ABVA** and **AVBVA** (Scheme 1), whose conjugation increased in sequence. We deemed that the increased conjugation would lead to the low-energy region emission. To the best our knowledge, there is no report on the organogel with the emission quite closing to NIR region, which would have potential applications in biological imaging. It was

found that **ABVA** and **AVBVA** without traditional gelation groups could form stable organogels in the mixed solvents containing 1,4-dioxane. The fluorescence emission of xerogel-based films generated from **ABVA** and **AVBVA** emerged at 710 nm and 745 nm, respectively. Interestingly, the emission of the xerogel-based films of **ABVA** and **AVBVA** could be quenched by *n*-propylamine and *n*-butylamine vapors, accompanied with the appearance of new strong emission at ca. 560 nm on account of the decomposition of the boron complexes. Other selected organic amines only quenched the emission of films because of the weak interactions between amines and boron complexes. Therefore, the nanofibers generated from nonclassical gelators of some difluoroboron β-diketonate complexes via organogelation could detect gaseous aliphatic primary amines with high performance.

Synthesis

The synthetic routes for **ABA**, **ABVA** and **AVBVA** were shown in Scheme 1. Firstly, compounds **1**-**5** were prepared according to the reported procedures.[21] The Claisen condensation reaction between compounds **1** and **2** was carried out in anhydrous THF in the presence of sodium hydride to afford the intermediate of β-diketone, which was not further purified and complexed with boron trifluoride-diethyl etherate

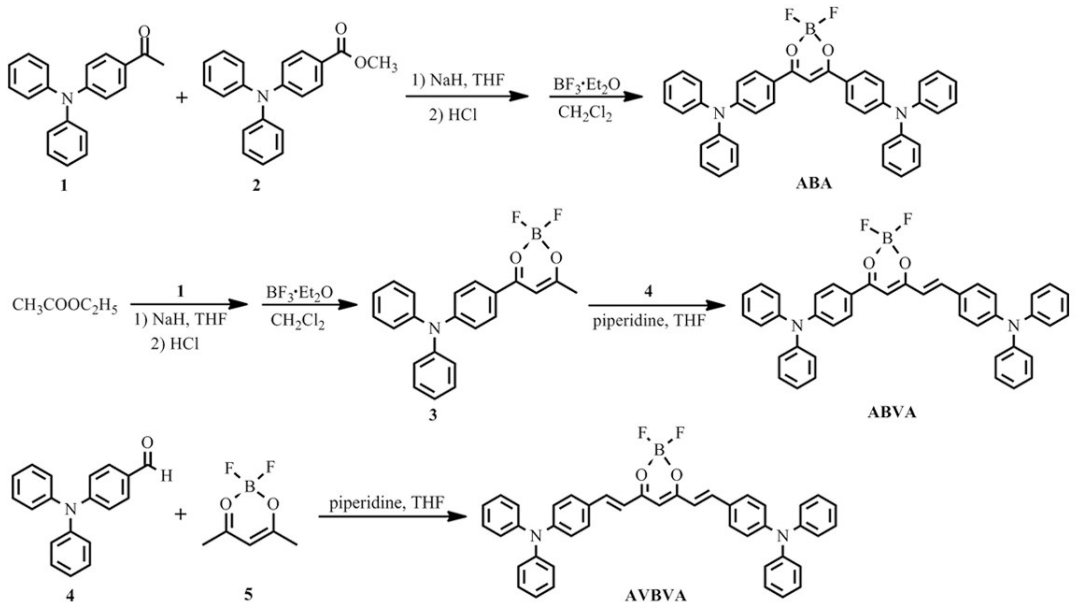

Scheme 1 Synthetic routes for difluoroboron β-diketonate complexes **ABA, ABVA** and **AVBVA**.

directly in anhydrous CH_2Cl_2 to yield complex **ABA** in a yield of 52%. Similarly, the Claisen condensation reaction between compound **1** and ethyl acetate, followed by complexed with boron trifluoride-diethyl etherate, afforded compound **3** in a yield of 46%. Then, the Knoevenagel condensation reaction between compounds **3** and 4-(diphenylamino)benzaldehyde **4** in the presence of piperidine in anhydrous THF gave **ABVA** in a yield of 27%. Complex **AVBVA** was synthesized via the Knoevenagel condensation reaction between compounds **4** and **5** in a yield of 45%. The target complexes were characterized by ^{1}H NMR, ^{13}C NMR, FT-IR and MALDI-TOF mass spectrometries. In ^{1}H NMR spectrum of **ABVA**, the coupling constants of peaks at 7.98 ppm and 6.60 ppm were 16.0 Hz, meaning the *trans*-form of vinyl group. Similarly, we deduced that the vinyl groups in **AVBVA** also existed in *trans*-forms.

Results and discussion

Photophysical properties in solutions

The UV-vis absorption and fluorescence emission spectra of **ABA**, **ABVA** and **AVBVA** in different solvents were shown in Figure 1, and the corresponding photophysical data were summarized in Table S1†. It was clear that the absorption band of **ABA** appeared at 488 nm in cyclohexane, which red-shifted to ca. 501 nm in toluene, THF and acetone with moderate polarity and to 516 nm in DMSO with high polarity (Figure 1a, Table S1†). It suggested that the maximal absorption band of **ABA** could be ascribed to charge-transfer (CT) transition. In the cases of **ABVA**, the structured absorption peaks emerged at 501 nm and 527 nm in cyclohexane, and only one strong absorption band was detected in other solvents. For example, the absorption of **ABVA** appeared at 539 nm and 560 nm in THF and in DMSO, respectively (Figure 1b). Similar solvent-dependent absorption spectral changes were also observed for **AVBVA** (Figure 1c). Therefore, the absorption bands for **ABVA** and **AVBVA** were also originated from CT transitions. It should be noted that with increasing the molecular conjugated length of difluoroboron β-diketonate complexes, the absorption bands red-shifted obviously, for instance, the absorption of **ABA**, **ABVA** and **AVBVA** emerged at 500 nm,

541 nm and 574 nm in toluene. As shown in Figure 1d-f, the emission bands of **ABA**, **ABVA** and **AVBVA** red-shifted obviously with increasing solvent polarities. For example, the emission peak of **ABVA** was located at 533 nm in cyclohexane and 678 nm in DMSO. Thus, the Stokes shifts increased obviously with increasing solvent polarities, and they were 892 cm^{-1} and 3108 cm^{-1} in cyclohexane and DMSO, respectively. Besides, **ABVA** was highly emissive in toluene with a fluorescence quantum yield (Φ_F) of 0.70 using fluorescein in 1 M NaOH (Φ_F = 0.95) as the standard, but it was almost non-emissive in DMSO. The red-shift and the broadening of the emission bands, as well as the decrease of Φ_F for **ABVA** with increasing solvent polarities illustrated the occurrence of ICT. Similarly, the emission of **ABA** and **AVBVA** was also originated from ICT transitions. Meanwhile, we found that the emission bands of **ABVA** and **AVBVA** appeared in low energy region compared with **ABA** on account of their extended conjugation. For example, the emission of **ABA** was located at 552 nm and red-shifted to 590 nm and 621 nm for **ABVA** and **AVBVA** in toluene. It was noticed that the Φ_F values of **ABA** and **AVBVA** reached 0.97 and 0.82, respectively, in toluene, meaning high emissive in non-polar solvents of the synthesized difluoroboron β-diketonate complexes.

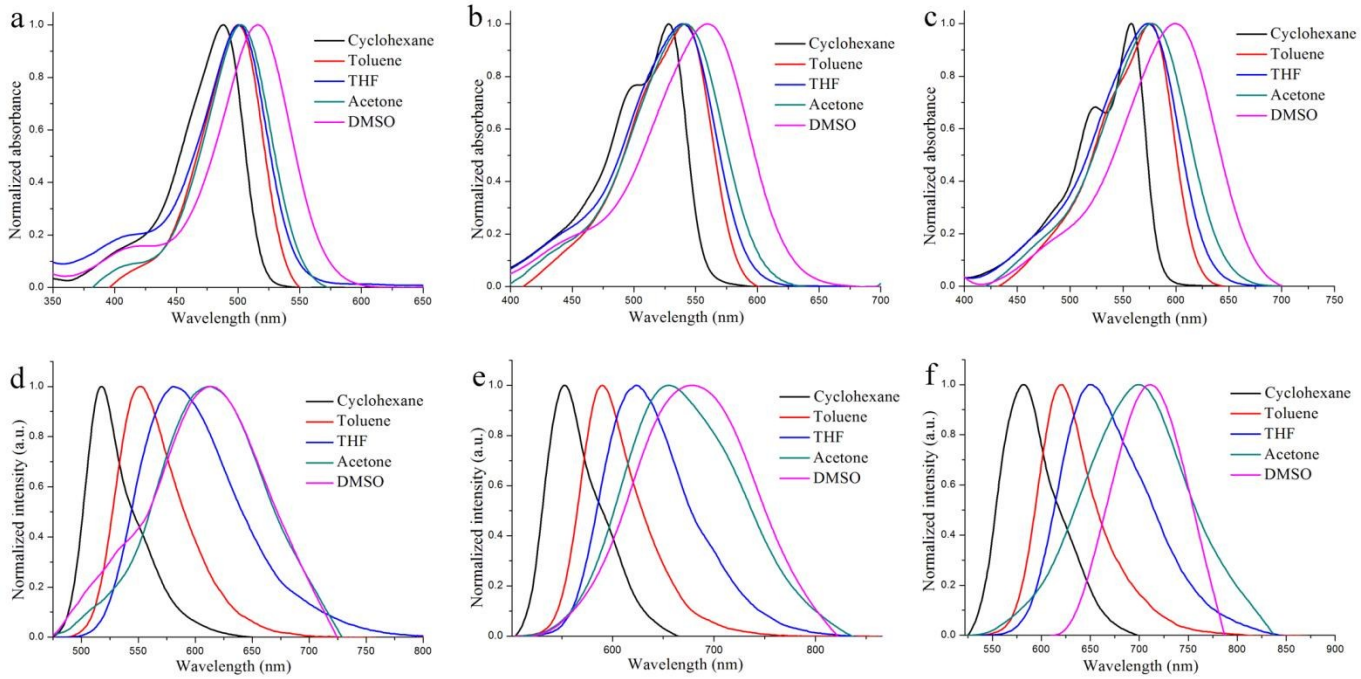

Figure 1. Normalized UV-vis absorption spectra of **ABA** (a), **ABVA** (b) and **AVBVA** (c), and fluorescence emission spectra of **ABA** (d, λ_{ex} = 515 nm), **ABVA** (e, λ_{ex} = 560 nm) and **AVBVA** (f, λ_{ex} = 598 nm) in different solvents (2.0×10^{-6} M).

Electrochemical properties

The cyclic voltammograms of the synthesized difluoroboron β-diketonate complexes were shown in Figure S1†. The well-defined reversible reduced peaks with half-wave potentials of -0.93 V, -0.73 V and -0.72 V versus ferrocenium/ferrocene were detected for **ABA**, **ABVA** and **AVBVA**, respectively (Table 1). The reductive half-wave potentials reduced in the order of **AVBVA** > **ABVA** > **ABA** because the conjugation increased with increasing the number of vinyl group. The HOMO and LUMO energy levels were calculated using the empirical equations: E_{LUMO} = - (E_{red} + 4.8) and E_{HOMO} = E_{LUMO} - E_g, in which E_g was estimated from the onset of the absorption spectrum (E_g = 1240/λ_{onset}). The HOMO energy levels of **ABA**, **ABVA** and **AVBVA** were -5.32 eV, -5.31 eV and -5.18 eV, respectively, and the LUMO energy levels of **ABA**, **ABVA** and **AVBVA** were estimated to be -3.11 eV, -3.31 eV and -3.32 eV, respectively (Table 1). The HOMO-LUMO energy gap of **AVBVA** was only 1.86 eV, so that we found its absorption as well as emission bands emerged in low energy region.

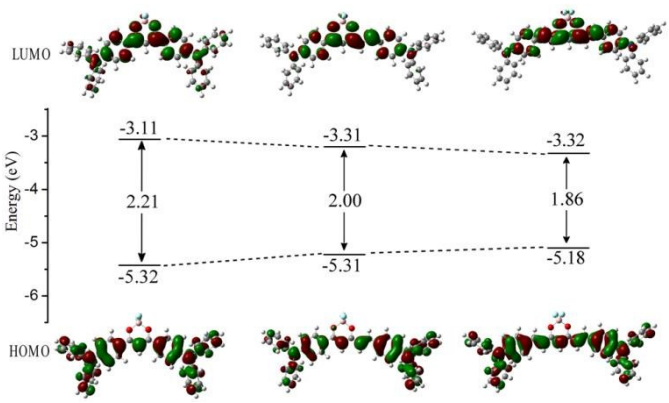

Figure 2. Energy levels and molecular orbital surfaces in the optimized ground-state structures of **ABA**, **ABVA** and **AVBVA**, in which hexadecyl groups were omitted.

Table 1 Electrochemical data and HOMO/LUMO energy levels of **ABA**, **ABVA** and **AVBVA**.

Complex	E_{onset}^{red} (V)[a]	E_{HOMO} (eV)[b]	E_{LUMO} (eV)[b]	E_g (eV)[c]	E_{HOMO} (eV)[d]	E_{LUMO} (eV)[d]
ABA	-0.93	-5.32	-3.11	2.21	-5.32	-2.48
ABVA	-0.73	-5.31	-3.31	2.00	-5.23	-2.61
AVBVA	-0.72	-5.18	-3.32	1.86	-5.17	-2.69

[a] E_{onset}^{red} (V) = onset reduction potential; Fc^+/Fc was used as external reference. [b] $E_{LUMO} = -(E_{onset}^{red} + 4.18)$; $E_{HOMO} = E_{LUMO} - E_g$. [c] Determined from the onset of the absorption at the lower energy band edge ($E_g = 1240/\lambda_{onset}$). [d] Calculated data.

Theoretical calculation

To gain an insight into the electronic structures of **ABA**, **ABVA** and **AVBVA**, quantum chemical calculations were performed by density functional theory calculations at the B3LYP/6-31G(d) level. As shown in Figure 2, we could find that the LUMOs of **ABA**, **ABVA** and **AVBVA** were mainly distributed in the central difluoroboron β-diketone units. The HOMO of **AVBVA** mainly distributed at the terminal triphenylamine units, suggesting D-A-D type π-skeleton. The molecular orbital distributions of **ABA** and **ABVA** were similar to that of **AVBVA**. That was why ICT would take place for the three complexes. In addition, the calculated HOMO energy levels of **ABA**, **ABVA** and **AVBVA** were similar to those based on electrochemical results. Although the calculated LUMO energy levels were higher than the data from electrochemical results, they were in the same order of **AVBVA** < **ABVA** < **ABA**.

Gelation properties

The gelation properties of **ABA**, **ABVA** and **AVBVA** were tested in the selected solvents by means of the "stable to inversion of a test tube" method.[21] The results were listed in Table 2. The gels could be gained from **ABVA** and **AVBVA** in the mixed solvents containing 1,4-dioxane, such as 1,4-dioxane/cyclohexane (v/v = 1/4, Figure S2†), 1,4-dioxane/*n*-hexane (v/v = 1/2), 1,4-dioxane/*n*-heptane (v/v = 1/2), 1,4-dioxane/*n*-octane (v/v = 1/1), after the hot solutions were first stimulated by ultrasound for few seconds and were then cooled to room temperature. The critical gelation concentrations (CGC) of **ABVA** and **AVBVA** depended on the solvents and varied in the range of 4.0-7.7 mmol/L and 6.8-33.3 mmol/L, respectively. The obtained gels of **ABVA** were stable for several months at room temperature, while the gels of **AVBVA** disappeared after standing at room temperature for several hours. It indicated that **ABVA** exhibited better gelation abilities than **AVBVA**. The formed gels could be transformed into solutions upon heating, which could recover to organogels upon stimulation by ultrasound, followed by cooling. However, complex **ABA**, in which two triphenylamines were directly linked to difluoroboron β-diketone unit, could not form any gel in the selected solvents due to its good solubility. The introduction of vinyl group between triphenylamine and difluoroboron β-diketone moieties would increase the conjugation degree, so that π-π interaction would play a role in the gel formation of **ABVA** and **AVBVA**, which will be discussed below. Additionally, we deemed that the reason for better gelation ability of **ABVA** than **AVBVA** was that the strong π-π interaction between **AVBVA** molecules might lead to high crystallization, leading to poor gelation ability. Therefore, the gelation ability of the nonclassical π-gelators could be tuned by

Table 2 Gelation abilities of complexs **ABA**, **ABVA** and **AVBVA** in organic solvents.

Solvent	**ABA** (CGC[a]/mM)	**ABVA**	**AVBVA**
n-Hexane	I	I	I
Cyclohexane	I	I	I
n-Heptane	I	I	I
n-Octane	I	I	I
tert-Amyl alcohol	S	S	S
1,4-Dioxane	S	S	S
Chloroform	S	S	S
Chlorobenzene	S	S	S
DMF	S	S	S
DMSO	S	S	S
THF	S	S	S
1,4-Dioxane/*n*-Hexane (v/v = 1/2)	S	G (7.1)	G (9.1)
1,4-Dioxane/Cyclohexane (v/v = 1/4)	S	G (4.0)	G (6.8)
1,4-Dioxane/*n*-Heptane (v/v = 1/3)	S	G (8.7)	PG
1,4-Dioxane/*n*-Heptane (v/v = 1/2)	S	PG	G (16.7)
1,4-Dioxane/*n*-Octane (v/v = 1/2)	S	G (7.7)	PG
1,4-Dioxane/*n*-Octane (v/v = 1/1)	S	PG	G (33.3)

I: insoluble; P: precipitate; PG: partly gel; S: soluble; G: gel.
[a] CGC: critical gelation concentration.

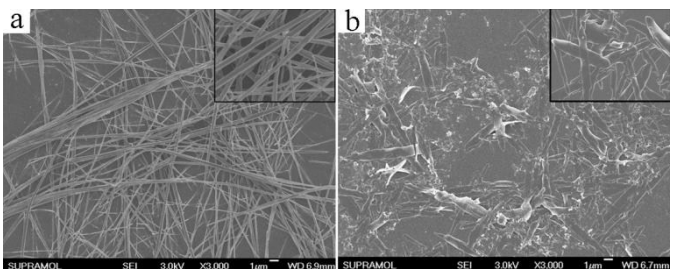

Figure 3. SEM images of xerogels **ABVA** (a) and **AVBVA** (b) obtained from 1,4-dioxane/cyclohexane (v/v = 1/4).

the strength of π-π interaction, and the balanced π-π interaction would be yielded from moderate conjugation degree and then promoted the gel formation. The morphologies of the xerogels **ABVA** and **AVBVA** obtained from 1,4-dioxane/cyclohexane (v/v = 1/4) were observed by SEM investigation (Figure 3). We could find that lots of straight and long fibers in diameters of ca. 200-500 nm were formed in the xerogel **ABVA**. However, **AVBVA** self-assembled into short and thick rods with diameters of 0.5-1.0 μm. Thus, the formed 3D networks consisting lots of nanofibers made the gel of **ABVA** more stable than the gel of **AVBVA**.

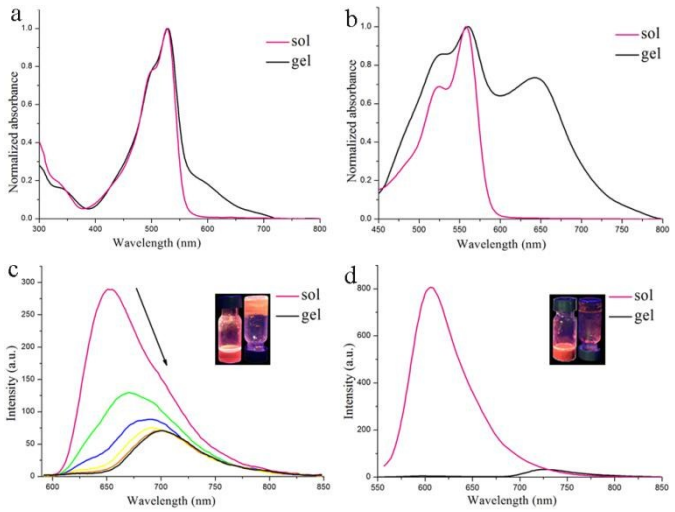

Figure 4. Normalized UV-vis absorption spectra of **ABVA** (a) in 1,4-dioxane/cyclohexane (v/v = 1/4, pink line for the solution with a concentration of 2.0×10^{-6} M and black line for the gel with a concentration of 4.0×10^{-3} M) and **AVBVA** (b) in 1,4-dioxane/cyclohexane (v/v = 1/4, pink line for the solution with a concentration of 2.0×10^{-6} M and black line for the gel with a concentration of 6.8×10^{-3} M); Time-dependent fluorescence emission spectra of **ABVA** (c) upon cooling the hot solution, which was first stimulated by ultrasound, to room temperature, in 1,4-dioxane/cyclohexane (v/v = 1/4, 4.0×10^{-3} M); Fluorescence emission spectra of **AVBVA** (d) in 1,4-dioxane/cyclohexane (v/v = 1/4, pink line for the solution with a concentration of 2.0×10^{-6} M and black line for the gel with a concentration of 6.8×10^{-3} M). The excitation wavelength is 550 nm.

In order to reveal the driving force for the gelation, the UV-vis absorption and fluorescence emission spectra of **ABVA** and **AVBVA** in solutions and in gel phases were compared. As shown in Figure 4a, the maximal absorption peaks of **ABVA** in solution and in gel state were both located at ca. 528 nm, but a new absorption peak at 600 nm emerged in gel state. It indicated that π-π interaction happened in the gel of **ABVA**.[23] Unlike **ABVA**, the maximal absorption peaks of **AVBVA** was little red-shifted in gel state compared with in solution and a new strong absorption band at 650 nm emerged in gel state. We speculated that the new strong absorption bands were originated from strong π-π interaction due to the larger conjugation degree of **AVBVA**. It also indicated that π-π interaction played a key role in gel formation of **AVBVA**.[23] Moreover, it suggested that the balanced π-π interaction could lead to the gel formation of nonclassical π-gelators without alkyl chain and H-bonding units.

Figure 4c showed the time-dependent fluorescence emission spectra of **ABVA** upon cooling the hot solution, which was first stimulated by ultrasound, to room temperature. It was clear that **ABVA** emitted strong red light with an emission at 653 nm in hot solution. During the gelation process, the emission band red-shifted gradually, accompanying with the decrease of the emission intensity. However, the organogel of **ABVA** still exhibited strong red emission centered at 702 nm (inset in Figure 4c). Similarly, **AVBVA** gave a strong emission at 606 nm in hot solution, which red-shifted to 730 nm and decreased dramatically in gel state. Such aggregation-caused quenching of the emission further suggested that π-aggregates were formed in organogels.[24]

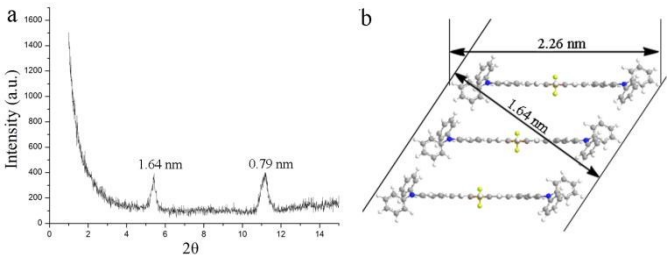

Figure 5. (a) X-ray diffraction pattern of the xerogel **AVBVA** deposited on glass slide and (b) Schematic illustration of the layered structure with the period of 1.64 nm in xerogel **AVBVA**.

Figure 5a showed the XRD pattern of xerogel **AVBVA** obtained from 1,4-dioxane/cyclohexane (v/v = 1/4), and we could find two obvious diffraction peaks corresponding to *d*-spacing of 1.64 nm and 0.79 nm, which were in a ratio of ca. 1:1/2. It indicated a lamellar organization formed in the aggregates of **AVBVA** with an interlayer distance of 1.64 nm. To reveal the molecular packing model, the optimized configuration of **AVBVA** was evaluated by the semiempirical (AM1) calculations. As shown in Figure 5b, the central difluoroboron β-diketone unit and vinyl units lay in the same plane, implying a good planarity. As a result, the extended width of **AVBVA** was calculated to be 2.26 nm, which suggested that the stacking mode in xerogel **AVBVA** adopted a tilted layered structure (Figure 5b). The XRD pattern of xerogel **ABVA** obtained from 1,4-dioxane/cyclohexane (v/v = 1/4) gave three diffraction peaks corresponding to *d*-spacing of 1.47 nm, 0.91 nm and 0.85 nm, respectively (Figure S3†). It meant that the molecules **ABVA** arranged into ordered structures in xerogel although it was difficult to deduce the molecular packing mode.

Xerogel-based film for detecting organic amine vapors

We have found in our previous work that the emission of nanofibers-based films fabricated from difluoroboron β-diketonate complexes could be quenched significantly by gaseous amines, so the sensory properties of the obtained organogel nanofibers-based films of **ABVA** and **AVBVA** towards amines were investigated. Interestingly, we found that the emission intensity at 710 nm for **ABVA** in nanofibers-based film decreased gradually with increasing the concentration of *n*-

propylamine vapor (Figure 6). When the concentration of *n*-propylamine vapor increased to 1.3×10^5 ppm, a new emission peak at 591 nm emerged. With further increasing the

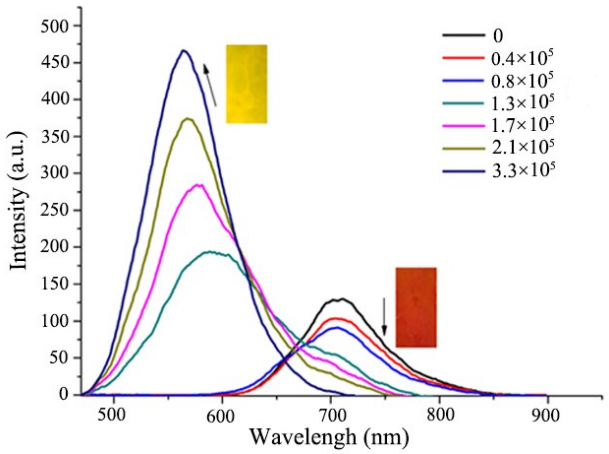

Figure 6. Fluorescence emission spectra of the xerogel-based film of **ABVA** upon exposure to *n*-propylamine in different concentrations (ppm) for 30 s (λ_{ex} = 360 nm). Insets: the xerogel films before and after exposed to saturated *n*-propylamine vapor under UV irradiation.

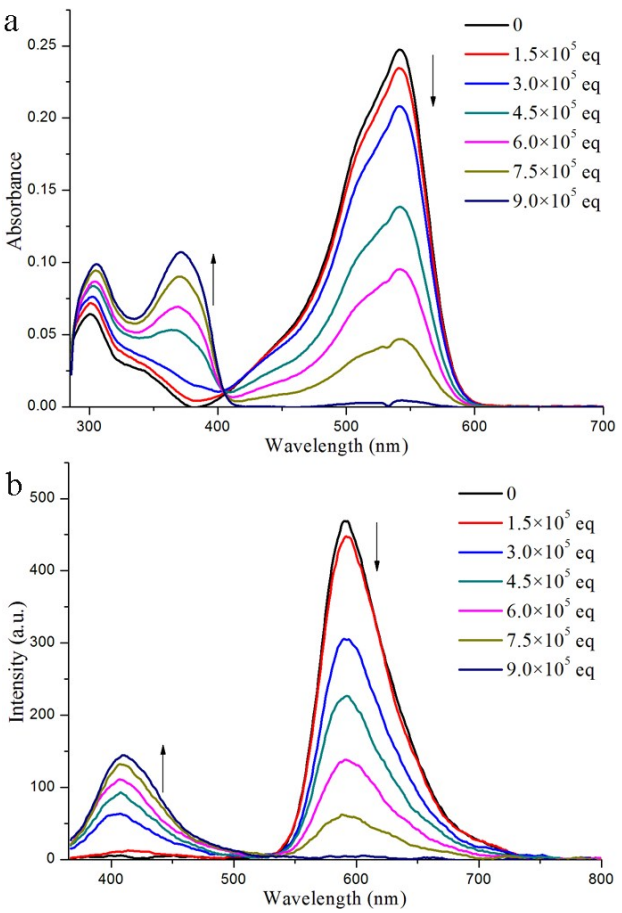

Figure 7. UV-vis absorption (a) and fluorescence emission (b, λ_{ex} = 360 nm) spectra of **ABVA** in toluene (2.0×10^{-6} M) upon adding different amount of *n*-propylamine.

concentration of *n*-propylamine vapor, the new emission peak blue-shifted gradually. When the film was exposed to saturated *n*-propylamine vapor (3.3×10^5 ppm) for 30 s, the emission peak at 710 nm disappeared completely and the new emission peak blue-shifted to 564 nm. At the same time, the emitting color of film changed from dark red to bright yellow (the insets of Figure 6), so the film based on nanofibers of **ABVA** could sense *n*-propylamine vapor by naked eyes.

In order to understand the fluorescence sensory mechanism of **ABVA** in the nanofibers-based film towards gaseous *n*-propylamine, the UV-vis absorption and fluorescence emission spectral titration experiments were performed. As shown in Figure 7b, the emission peak at 592 nm for **ABVA** in toluene reduced gradually with the increasing amount of *n*-propylamine. A new emission at 415 nm emerged when the equiv. of *n*-propylamine reached 1.5×10^5 versus fluorescent probe, and its intensity increased gradually upon adding more *n*-propylamine. When 9.0×10^5 equiv. of *n*-propylamine was added, we could only find one emission band at 410 nm. It was clear that the fluorescence spectral changes for **ABVA** induced by *n*-propylamine in toluene and in xerogel-based film were similar, so was the sensing mechanism. Figure 7a showed that the maximal absorption peak at 541 nm for **ABVA** decreased gradually with the increasing amount of *n*-propylamine, accompanying with the appearance of new absorption at 372 nm. When the equiv. of *n*-propylamine increased to 9.0×10^5 versus **ABVA**, the absorption at 541 nm disappeared completely. The isobestic point at 404 nm was observed, suggesting new species was yielded from **ABVA** induced by *n*-propylamine. In addition, we also found similar UV-vis absorption spectral changes for the xerogel-based film of **ABVA** upon exposure to *n*-propylamine (Figure S4†), further suggesting similar sensory mechanisms in solution as well as in xerogel-based film. To verify this speculation, ^{1}H NMR spectra of **ABVA** in $CDCl_3$ before and after adding *n*-propylamine were compared. As shown in Figure S5, two new signals at 5.60 ppm and 11.37 ppm were found when excess of *n*-propylamine was added. The new signal at 11.37 ppm was probably assigned to the hydrogen in hydroxyl group of the enol form for β-diketone and another one at 5.60 ppm may be ascribed to the hydrogen in methylene in β-diketone. Moreover, when a drop of D_2O was added to the above system containing **ABVA** and *n*-propylamine in $CDCl_3$, the signal at 11.37 ppm disappeared. It further illustrated that it was originated from active hydrogen. Therefore, we suggested that *n*-propylamine could attract electron-deficient boron unit in the complex to lead to the decomposition of difluoroboron β-diketonate, and β-diketone might probably one of the main deposited product. Additionally, the UV-Vis absorption and fluorescence spectral changes of **AVBVA** in xerogel-based film were similar to those of **ABVA** upon exposure to *n*-propylamine vapor (Figure S6†). It meant that the sensory mechanism of **AVBVA** in response to *n*-propylamine was same as that of **ABVA**.

Moreover, we also studied the fluorescence response behaviors of **ABVA** in xerogel-based film upon exposure to other amines and pyridine. As shown in Figure S7†, the

fluorescence spectral changes of **ABVA** in xerogel-based film induced by *n*-butylamine were similar to *n*-propylamine, so we deemed that *n*-butylamine could also decompose **ABVA**. However, the other selected amines (such as triethylamine, tributylamine, aniline and cyclohexylamine) and pyridine could only quench the emission of **ABVA** in the film to various extents, and no new emission peak emerged, due to the weak interactions between amine and the boron complex unit in **ABVA**.[19b] Therefore, the nanofibers-based film fabricated via the organogelation of nonclassical organogelators **ABVA** and **AVBVA** could be used as fluorescence sensory materials to detect aliphatic primary amine vapors selectively by naked eyes.

Conclusions

Three new D-A-D type triphenylamine functionalized difluoroboron β-diketonate complexes **ABA**, **ABVA** and **AVBVA** were synthesized. It was found that **ABVA** and **AVBVA**, in which one triphenylamine unit or two triphenylamine units were linked to difluoroboron β-diketonate by vinyl spacer, exhibited gelation ability in some mixed solvents containing 1,4-dioxane. They were nonclassical organogelators without long alkyl chains and hydrogen-bonded units. The UV-vis absorption and fluorescence emission spectra of **ABVA** and **AVBVA** in solutions and in gel phases revealed that π-π interaction played an important role in gel formation. Moreover, the emission of **ABVA** and **AVBVA** in xerogels appeared closing to NIR region. Interestingly, the vapors of *n*-propylamine and *n*-butylamine could quench the emission of **ABVA** and **AVBVA** in xerogel-based films, accompanied with the appearance of new strong emission at ca. 560 nm. Therefore, the emitting colors of the films changed from dark red to bright yellow. The UV-vis absorption titration experiment and ^{1}H NMR spectral change for **ABVA** upon adding *n*-propylamine illustrated that the aliphatic primary amines could lead to the deposition of difluoroboron β-diketonate complexes. Therefore, this kind of fluorescent organogels could be used as probes to detect aliphatic primary amines selectively.

Experimental section

Measurement and characterizations

^{1}H NMR and ^{13}C NMR spectra were recorded with a Mercury Plus instrument at 400 MHz and 100 MHz in $CDCl_3$ in all cases. FT-IR spectra were recorded with a Nicolet-360 FT-IR spectrometer by incorporation of samples into KBr disks. UV-vis absorption spectra were obtained on a Shimadzu UV-3100 spectrophotometer. Fluorescent emission spectra were obtained on a Cary Eclipse fluorescence spectrophotometer. Cyclic voltammetry spectra were measured on a CHI 604C voltammetric analyzer with a scan rate at 50 Mv/s. A three electrode configuration was used for the measurement: a platinum button as the working electrode, a platinum wire as the counter electrode, and a saturated calomel electrode (SCE) as the reference electrode. The solution of $(C_4H_9)_4NBF_4$ in CH_2Cl_2 (0.1 M) was used as the supporting electrolyte. Mass spectra were obtained with Agilent 1100 MS series and AXIMA CFR MALDI-TOF (Compact) mass spectrometers. XRD patterns were obtained on an Empyrean X-ray diffraction instrument. Scanning electron microscopy (SEM) was performed on JEOL JSM-6700F (operating at 5 kV). The samples were prepared by casting the organogels on silicon wafers and dried at room temperature, followed by coating with gold.

Preparation of the organogels and xerogel-based films

A clear solution of **ABVA** or **AVBVA** in 1,4-dioxane/cyclohexane (v/v = 1/4) was obtained by heating. After the hot solution was suffered a sonification for 10 s, followed by aging for 10 min at room temperature, the gel was formed. After diluting the gel of **ABVA** or **AVBVA** into a "poor" solvent of *n*-hexane, well-dispersed nanofibers were produced. The mesh-like films were fabricated after casting the nanofibers in *n*-hexane onto the substrates, followed by the natural evaporation of the solvent.

Investigation on the fluorescence sensory properties

The sensory investigations for the xerogel-based films of **ABVA** and **AVBVA** were carried out at 25℃. Firstly, the organic amine vapors and other analytes at a certain concentration were obtained by diluting the saturated vapors with nitrogen, and then injecting them into a quartz cell (10 mm in width) containing the film. The changes in the emission intensity and wavelength were recorded after injection of the organic amine or other interference vapors for 30 s.

Materials

CH_2Cl_2 was dried over calcium hydride. THF was dried over sodium and diphenyl ketone. The other reagents were used as received without further purification.

Synthesis

4,6-bis(4-(diphenylamino)phenyl)-2,2-difluoro-2H-1,3,2-dioxaborinin-1-ium-2-uide (ABA)

1-(4-(Diphenylamino)phenyl)ethanone **1** (0.5 g, 1.74 mmol) and methyl 4-(diphenylamino)benzoate **2** (0.53 g, 1.74 mmol) were dissolved in dry THF (20 mL) under an atmosphere of nitrogen. Then, NaH (0.1 g, 4.17 mmol) was added. After the mixture was stirred at 60 °C for 24 h, followed by poured into ice water (200 mL), HCl (6 M, 5 mL) was added to neutralize excess NaH. The mixture was extracted with CH_2Cl_2 (3 × 50 mL), and the organic phase was combined and dried over anhydrous magnesium sulfate. After removal of solvent, the residue was used directly in the next step without purification. The solution of the β-diketone of 1,3-bis(4-(diphenylamino)phenyl)-3-hydroxyprop-2-en-1-one in dry dichloromethane (50 mL) was heated to reflux under an atmosphere of nitrogen, excess $BF_3{\cdot}Et_2O$ (0.5 mL) was added. The mixture was refluxed for 2 h. After the solvent was removed, the residue was purified by column chromatography (silica) using petroleum ether/CH_2Cl_2 (v/v = 1/1) as eluent, followed by recrystallization from the mixed solvent of CH_2Cl_2

and light petroleum to afford **ABA** as dark red solid in a yield of 48 %. m.p.:134.0-136.0 °C; ^{1}H NMR (400 MHz, $CDCl_3$), δ (ppm): 7.95 (d, J = 8 Hz, 4H), 7.39 (t, $J_1 = J_2 = 8$ Hz, 8H), 7.25-7.21 (m, 12H), 7.01 (d, J = 4Hz, 4H), 6.90 (s, 1H) (Figure S8†); ^{13}C NMR (100 MHz, $CDCl_3$) δ (ppm): 178.87, 153.62, 145.73, 130.36, 129.85, 126.50, 125.58, 123.41, 118.91, 91.01, (Figure S9†); MALDI-TOF MS: m/z: calcd: 606.2; found: 588.4 $[M-F+H]^+$ (Figure S10†); FT-IR (KBr, cm^{-1}): 3442, 1542, 1481, 1338, 1245, 1180, 1033, 755, 701, 511.

6-(4-(diphenylamino)phenyl)-2,2-difluoro-4-methyl-2H-1,3,2-dioxaborinin-1-ium-2-uide (3)

Compound **1** (2.0 g, 6.96 mmol) and NaH (0.25 g, 10.44 mmol) was added in dry THF (20 mL). Then, ethyl acetate was added slowly under the ice bath. After the mixture was stirred in an ice bath for 2 h, HCl (6 M, 5 mL) was added to neutralize excess NaH. Then, the mixture was poured into water (200 mL), and extracted with CH_2Cl_2 (3 × 50 mL). The organic phase was washed with brine and dried with anhydrous magnesium sulfate. After the solvent was removed, the residue was used directly in the next step without purification. The solution of the crude intermediate of (Z)-1-(4-(diphenylamino)phenyl)-3-hydroxybut-2-en-1-one in dry dichloromethane (30 mL) was heated to reflux under an atmosphere of nitrogen, excess BF_3·Et_2O (1.8 mL) was added. The mixture was refluxed for 2 h. After the solvent was removed, the residue was purified by column chromatography using petroleum ether/CH_2Cl_2 (v/v = 1/1) as eluent. Yellow solid **3** was obtained in a yield of 32%. ^{1}H NMR (400 MHz, $CDCl_3$), δ (ppm): 7.87 (d, J = 8 Hz, 2H), 7.38 (t, J = 8 Hz, J = 8 Hz, 4H), 7.25-7.18 (m, 6H), 6.94 (d, J = 8 Hz, 2H), 6.36 (s, 1H), 2.32 (s, 3H) (Figure S11†); ^{13}C NMR (100 MHz, $CDCl_3$) δ (ppm): 188.19, 180.90, 154.51, 145.31, 131.22, 129.93, 126.70, 126.01, 121.48, 118.31, 95.91, 24.34 (Figure S12†); MALDI-TOF MS: m/z: calcd: 377.0; found: 378.3 $[M+H]^+$ (Figure S13†).

(E)-6-(4-(diphenylamino)phenyl)-4(4(diphenylamino)styryl)-2,2-difluoro-2H-1,3,2-dioxaborinin-1-ium-2-uide (ABVA)

Compounds **3** (0.45 g, 1.2 mmol) and 4-(diphenylamino)benzaldehyde **4** (0.33 g, 1.2 mmol) was dissolved in dry THF (20 mL). Then, four drops of piperidine were added. The mixture was stirred at the room temperature for 4 h. After the solvent was removed, the residue was purified by column chromatography (silica) using petroleum ether/CH_2Cl_2 (v/v = 1/10) as eluent, followed by recrystallization from the mixed solvent of CH_2Cl_2 and light petroleum to afford **ABVA** as black solid in a yield of 65 %. m.p.:144.0-146.0 °C. ^{1}H NMR (400 MHz, $CDCl_3$), δ (ppm): 7.96 (d, J = 16 Hz, 1H), 7.89 (d, J = 8 Hz, 2H), 7.44 (d, J = 8 Hz, 2H), 7.39-7.30 (m, 8H), 7.23-7.12 (m, 12H), 6.97 (t, J = 8 Hz, J = 12 Hz, 4H), 6.57 (d, J = 16 Hz, 1H), 6.41 (s, 1H) (Figure S14†); ^{13}C NMR (100 MHz, $CDCl_3$) δ (ppm): 153.80, 151.08, 146.39, 145.61, 130.67, 130.52, 129.87, 129.66, 126.92, 126.57, 125.95, 125.71, 124.78, 123.03, 120.70, 118.73, 117.75, 96.51 (Figure S15†); MALDI-TOF MS: m/z: calcd: 632.0; found: 633.0 $[M+H]^+$ (Figure S16†). FT-IR (KBr, cm^{-1}):3446, 1590, 1541, 1487, 1383, 1336, 1296, 1173, 1000, 756, 698.

4,6-bis((E)-4-(diphenylamino)styryl)-2,2-difluoro-2H-1,3,2-dioxaborinin-1-ium-2-uide (AVBVA)

The synthetic method for **AVBVA** was similar to that for **ABVA** except using compounds **4** (2.5 g, 9.15 mmol) and 2,2-difluoro-4,6-dimethyl-2H-1,3,2-dioxaborinin-1-ium-2-uide **5** (0.54 g, 3.65 mmol) as reactants. The crude product was purified by column chromatography (silica) using petroleum ether/CH_2Cl_2 (v/v = 1/10) as eluent, followed by recrystallization from the mixed solvent of CH_2Cl_2 and light petroleum to afford **AVBVA** as black solid in a yield of 43%. m.p.:148.0-150.0 °C. ^{1}H NMR (400 MHz, $CDCl_3$), δ (ppm): 7.95 (d, J = 16 Hz, 2H), 7.43 (d, J = 8 Hz, 4H), 7.35-7.31 (m, 8H), 7.15 (t, J = 8 Hz, J = 8 Hz, 12H), 6.98 (d, J = 8 Hz, 4H), 6.52 (d, J = 16 Hz, 2H), 5.96 (s, 1H) (Figure S17†); ^{13}C NMR (100 MHz, $CDCl_3$) δ (ppm): 151.29, 146.29, 130.70, 129.68, 126.79, 126.02, 124.85, 120.54, 117.38, 101.75 (Figure S18†); MALDI-TOF MS: m/z: calcd: 658.0; found: 659.0 $[M+H]^+$ (Figure S19†). FT-IR (KBr, cm^{-1}):3460, 2353, 1591, 1525, 1286, 1149, 1003, 826, 749, 690.

Acknowledgements

This work was financially supported by the National Natural Science Foundation of China (21374041 and 21503090), the Open Project of State Key Laboratory of Supramolecular Structure and Materials (SKLSSM201615).

Notes and references

[a] State Key Laboratory of Supramolecular Structure and Materials, College of Chemistry, Jilin University, Changchun, P. R. China. E-mail: luran@mail.jlu.edu.cn

† Electronic Supplementary Information (ESI) available: ^{1}H NMR, ^{13}C NMR, MALDI/TOF MS and CV spectra; Photophysical data for target molecules; Fluorescent sensory properties. See DOI: 10.1039/x0xx00000x

[1] I. Akinori, G. X. Lin and J. E. Penner, *Atmospheric Environment*, 2015, **121**, 103-112.

[2] K. Matsumoto, Y. Yamamoto, H. Kobayashi, N. Kaneyasu and T. Nakano, *Atmospheric Environment*, 2014, **95**, 334-343.

[3] J. L. Pablos, S. Vallejos, A. Muñoz, M. J. Rojo, F. Serna, F. C. García and J. M. García, *Chem. - Eur. J.*, 2015, **21**, 8733-8736.

[4] C. Berbegal, I. Pardo and S. Ferrer, *J. Sci. Food Agric*, 2016, **96**, 1556-1561.

[5] G. I. Mohammed, A. S. Bashammakh, A. A. Alsibaai, H. Alwael and M.S. El-Shahawi, *Trends in Analytical Chemistry*, 2016, **78**, 84-94.

[6] J. Aneta, P. Anna, K. Sylwia, K. Marek and S. Edward, *J. Food Compos. Anal.*, 2016, **48**, 111-119.

[7] Y. Chen, K. Ma, T. Hu, B. Jiang, B. Xu, W. J. Tian, J. Z. Sun and W. K. Zhang, *Nanoscale*, 2015, **7**, 8939-8945.

[8] M. J. Dai, Y. L. Lin, H. C. Lin, H. W. Zan, K. T. Chang, H. F. Meng, J. W. Liao, M. J. Tsai, M. J. Tsai and H. R. Cheng, *Anal. Chem.*, 2013, **85**, 3110-3117.

[9] R. Adrover, D. Cocozzella, E. Ridruejo, A. Garc á and J. J. Podestá, *Dig. Dis. Sci.*, 2012, **57**, 189-195.

[10] (a) R. Pandeeswari and B. G. Jeyaprakash, *Sens. Actuators, B*, 2014, **195**, 206-214; (b) V. Talwar, O. Singh and R. C. Singh, *Sens. Actuators, B*, 2014, **191**, 276-282. (c) P. Dhivya, A. K. Prasad and M. Sridharan, *Ceram. Int.*, 2014, **40**, 409-415.

[11] (a) S. Grecoa, W. Danyszb, A. Zivkovic, R. Gross and H. Stark, *Anal. Chim. Acta*, 2013, **771**, 65-72; (b) X. E. Zhao, S.Y. Zhu, H. M. Yang, J. M. You, F. R. Song, Z. Q. Liu and S.Y. Liu, *J. Chromatogr. B*, 2015, **995-996**, 15-23; (c) J. Y. Hong, N. H. Park, M. S. Oh, H. S. Lee, H. S. Pyo and J. K. Hong, *J. Chromatogr. B*, 2013, **940**, 94-103.

[12] (a) A. R. Longstreet, M. Y. Jo, R. R. Chandler, K. Hanson, N. Q. Zhan, J. J. Hrudka, H. Mattoussi, M. Shatruk and D. T. McQuade, *J. Am. Chem. Soc.*, 2014, **136**, 15493-15496; (b) M. Gao, S. W. Li, Y. H. Lin, Y. Geng, X. Ling, L. C. Wang, A. J. Qin and B. Z. Tang, *ACS Sensor*, 2016, **1**, 179-184; (c) L. Q. Shi, Y. Y. Fu, D. F. Zhu, Y. X. Gao, Y. R. Wang, Q. G. He, H. M. Cao and J. G. Cheng, *Chem. Commun.*, 2014, **50**, 872-874; (d) M. Venkateswarulu, P. Gaur and R. R. Koner, *Sens. Actuators, B*, 2015, **210**, 144-148; (e) K. Wang, H. Yang, X. M. Qian, Z. Xue, Y. Q. Li, H. B. Liu and Y. L. Li, *Dalton Trans.*, 2014, **4**3, 11542-11547; (f) F. Q. Wang, C. F. Dong, C. M. Wang, Z. C. Yu, S. K. Guo, Z. C. Wang, Y. N. Zhao and G. D. Li, *New J. Chem.*, 2015, **39**, 4437-4444.

[13] B. Valeur, Molecular Fluorescence. *Principles and Applications*, Wiley VCH, Weinheim, 2002.

[14] Y. K. Che, X. M. Yang, S. Loser and L. Zang, *Nano. Lett.*, 2008, **8**, 2219-2223

[15] Y. K. Che, X. M. Yang, Z. X. Zhang, J. M. Zuo, J. S. Moore and L. Zang, *Chem. Commun.*, 2010, **46**, 4127-4129.

[16] S. Körsten and G. J.Mohr, *Chem. -Eur. J.*, 2011, **17**, 969-975.

[17] G. J. Mohr, D. Citterio, C. Demuth, M. Fehlmann, L. Jenny, C. Lohse, A. Moradian, T. Nezel, M. Rothmaier and U. E. Spichiger, *J. Mater. Chem.*, 1999, **9**, 2259-2264.

[18] H. N. Peng, L. P. Ding, T. H. Liu, X. L. Chen, L. Li, S. W. Yin and Y. Fang, *Chem. -Asian J.*, 2012, **7**, 1576-1582.

[19] (a) X. L. Liu, X. F. Zhang, R. Lu, P. C. Xue, D. F. Xu and H. P. Zhou, *J. Mater. Chem.*, 2011, **21**, 8756-8765; (b) X. F. Zhang, X. L. Liu, R. Lu, H. Zhang and P. Gong, *J. Mater. Chem.*, 2012, **22**, 1167-1172; (c) P. C. Xue, Q. X. Xu, P. Gong, C. Qian, A. M. Ren, Y. Zhang and R. Lu, *Chem. Commun.*, 2013, **49**, 5838-5840; (d) C. Qian, K.Y. Cao, X. L. Liu, X. F. Zhang, D. F. Xu, P. C. Xue and R. Lu, *Chin. Sci. Bull.*, 2012, **57**, 4264-4271; (e) P. C. Xue, B. Q. Yao, P. P. Wang, P. Gong, Z. Q. zhang and R. Lu, *Chem. -Eur. J.*, 2015, **21**, 17508 -17515.

[20] (a) X. C. Yang, R. Lu, T. H. Xu, P. C. Xue, X. L. Liu and Y. Y. Zhao, *Chem. Commun.*, 2008, 453–455; (b) X. C. Yang, R. Lu, F. Y. Gai, P. C. Xue and Y. Zhan, *Chem. Commun.*, 2010, **46**, 1088–1090; (c) X. F. Zhang, R. Lu, J. H. Jia, X. L. Liu, P. C. Xue, D. F. Xu and H. P. Zhou, *Chem. Commun.*, 2010, **46**, 8419–8421; (d) P. C. Xue, B. Q. Yao, J. B. Sun, Z. Q. Zhang and R. Lu, *Chem. Commun.*, 2014, **50**, 10284–10286; (e) J. Seo, J. W. Chung, I. Cho and S. Y. Park, *Soft Matter*, 2012, **8**, 7617–7622; (f) J. Lee, J. E. Kwon, Y. You and S. Y. Park, *Langmuir*, 2014, **30**, 2842–2851; (g) Z. Xie, V. Stepanenko, B. Fimmel and F. Würthner, *Mater. Horiz.*, 2014, **1**, 355–359; (h) E. Sheepwash, V. Krampl, R. Scopelliti, O. Sereda, A. Neels, and K. Severin, *Angew. Chem. Int. Ed.*, 2011, **50**, 3034 –3037; (i) Z. Ding, Q. Zhao, R. Xing, X. Wang, J. Ding, L. Wang and Y. Han, *J. Mater. Chem. C*, 2013, **1**, 786–792.

[21] (a) J. N. Weng, Q. B. Mei, Q. D. Ling, Q. L. Fan and W. Huang, *Tetrahedron*, 2012, **68**, 3129-3134; (b) Y. L. Fan, B. P. Lin, Y. Sun, X. H. Gong, H. Yang and X. Q. Zhang, *Polym. Chem*., 2013, **4**, 4245-4255; (c) M. Lian, Y.Yu, J. Zhao, Z. Huang, X.L. Yang, G. J. Zhou, Z. X. Wu and D. D. Wang, *J. Mater. Chem. C*, 2014, **2**, 9523-9535; (d) C. Z. Ran, X. Y. Xu, S. B. Raymond, B. J. Ferrara, K. Neal, B. J. Bacskai, Z. Medarova, and A. Moore, *J. Am. Chem. Soc.*, 2009, **131**, 15257-15261.

[22] (a) N. M. Sangeetha and U. Maitra, *Chem. Soc. Rev.*, 2005, **34**, 821-836; (b) S. K. Samanta, A. Pal and S. Bhattacharya, *Langmuir*, 2009, **25**, 8567-8578;

[23] S. Ghosh, X. Q. Li, V. Stepanenko, F. Würthner, *Chem. - Eur. J.*, 2008, **14**, 11343 - 11357.

[24] J. B. Birks, Photophysics of Aromatic Molecules, Wiley, London, 1970.

Graphic Abstract For:

Nanofibers generated from nonclassical organogelators based on difluoroboron β-diketonate complexes to detect aliphatic primary amine vapors

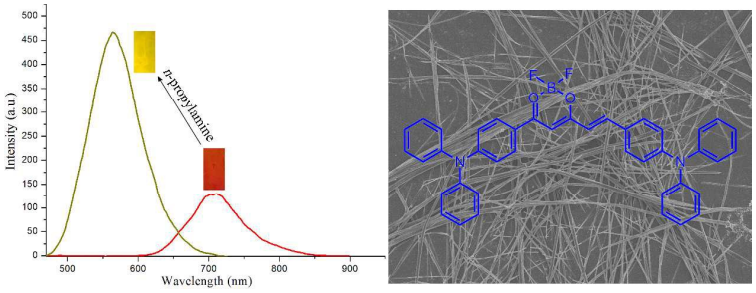

Narrow band gap nonclassical π-organogelators self-assembled into nanofibers for detecting primary amine vapors via the decomposition of difluoroboron β-diketonate complexes.